

Guiding center picture of magnetoresistance oscillations in rectangular superlattices

Rolf R. Gerhardt and Stephan D. M. Zwerschke

Max-Planck-Institut für Festkörperforschung, Heisenbergstrasse 1, D-70569 Stuttgart, Germany
(November 2, 2018)

We calculate the magneto-resistivities of a two-dimensional electron gas subjected to a lateral superlattice (LSL) of rectangular symmetry within the guiding-center picture, which approximates the classical electron motion as a rapid cyclotron motion around a slowly drifting guiding center. We explicitly evaluate the velocity auto-correlation function along the trajectories of the guiding centers, which are equipotentials of a magnetic-field dependent effective LSL potential. The existence of closed equipotentials may lead to a suppression of the commensurability oscillations, if the mean free path and the LSL modulation potential are large enough. We present numerical and analytical results for this suppression, which allow, in contrast to previous quantum arguments, a classical explanation of similar suppression effects observed experimentally on square-symmetric LSL. Furthermore, for rectangular LSLs of lower symmetry they lead us to predict a strongly anisotropic resistance tensor, with high- and low-resistance directions which can be interchanged by tuning the externally applied magnetic field.

73.40.-c, 73.50.Jt, 73.61-r

I. INTRODUCTION

Pronounced commensurability oscillations of the magnetoresistance of a two-dimensional electron gas (2D EG) subjected to a perpendicular magnetic field and a lateral superlattice, now also known as Weiss oscillations (WO), have first been observed on systems with a periodic modulation in one direction (1D).¹⁻³ Subsequent work on systems with a 2D lateral superlattice (LSL) showed that the modulation in the second direction tends to suppress the commensurability oscillations.⁴⁻⁸ The WO observed on samples with a 1D LSL, and their suppression in samples with a 2D LSL, were first explained by quantum mechanically. A 1D modulation broadens the Landau levels into bands of oscillatory width, with finite group velocity. This leads, in addition to the scattering induced magnetoconductivity (the so called “scattering conductivity”), to a “band conductivity” which vanishes if the Landau bands become flat.^{2,3,9} A modulation in the second lateral direction splits these Landau bands into narrow subbands with small group velocities, and, as a function of the magnetic flux per unit cell of the 2D LSL, a self-similar energy spectrum (“Hofstadter’s butterfly”) results.^{10,11} It has been argued that this subband splitting leads to a suppression of the band conductivity, if the modulation-induced width of the Landau bands is sufficiently large, and collision broadening effects are sufficiently weak.^{6,11} Experiments on samples with a weak 2D modulation and not too high mobility show indeed commensurability oscillations very similar to those observed in 1D LSLs, which are suppressed (and changed in character) with increasing modulation strength and mobility.^{7,8}

Soon after their discovery, Beenakker¹² explained the most prominent of the WO in an electrostatically defined 1D LSL classically, as resulting from an oscillatory $\mathbf{E} \times \mathbf{B}$ drift of the guiding centers (GCs) of cyclotron orbits, where the GC velocity plays the role of the group

velocity in the quantum treatment.¹³ The GC picture can be justified for weak modulations and intermediate strengths of the applied magnetic field.^{14,15} It has been used to calculate the resistivity for different analytical forms of electrostatic, magnetostatic and mixed modulations defining 1D or 2D LSLs.¹⁶ A clear classical picture for the suppression of the WO in 2D LSLs has, however, not been developed for nearly a decade, although direct numerical evaluations of the diffusion tensor on the basis of classical ballistic models indicated such a suppression.^{7,17}

Recently Grant *et al.*¹⁸ emphasized that the GCs move along the equipotential lines of an effective potential, determined by an average of the modulation fields over unperturbed cyclotron orbits.¹⁷ They argued that, in a 2D LSL of square symmetry, these equipotentials are closed, and that therefore the GC velocity averages to zero, resulting in a suppression of the WO, and they confirmed this conjecture by ballistic model calculation. Recent experiments demonstrate also, that an asymmetric 2D modulation leads to much stronger commensurability oscillations than a square-symmetric one does.¹⁹ While Grant *et al.*¹⁸ employed the GC picture to make the suppression of WO in 2D LSL plausible, they did not really use it as basis of their calculation. Moreover, they considered a strong modulation, so that their results are not directly comparable with previous predictions for weak modulation.¹⁶ A consistent evaluation of the GC approach, which is known to yield a very simple and intuitive picture of the WO in 1D LSLs, is so far not available for the case of 2D LSLs. The aim of the present work is to fill this gap.

In Sect. II we discuss the GC approach and its limitations. Based on a numerical evaluation of the diffusion tensor, we present in Sect. III simple analytical results for the conductivities of square and rectangular LSLs defined by harmonic electric and magnetic modulation fields. These results depend only on one (square LSL)

respectively two (rectangular LSL) parameters, which are determined by the (seven) modulation model parameters, the mean free path, and the average magnetic field. Illustrative examples are given, including a strongly anisotropic case in which the applied magnetic field can interchange the directions of high and low resistance. Mathematical details are given in two appendices.

II. THE GUIDING CENTER PICTURE

A. Heuristic definition

We consider a 2D EG in the x - y plane subjected to a strong homogeneous, perpendicular magnetic field $\mathbf{B}_0 = (0, 0, B_0)$ and a LSL defined by weak electric and magnetic modulation fields. The classical magnetoconductivity of this system can be calculated¹⁴ from the motion of electrons at the Fermi energy $E_F = (m/2)v_F^2$. Within the GC picture, this is assumed to be the superposition

$$\mathbf{r}(t) = \mathbf{r}_{\text{gc}}(t) + \mathbf{r}_{\text{cyc}}(t) \quad (1)$$

of a rapid cyclotron motion $\mathbf{r}_{\text{cyc}}(t) = R(\sin \alpha, -\cos \alpha)$ around a slowly moving guiding center $\mathbf{r}_{\text{gc}}(t)$, where $\alpha(t) = \omega_0 t + \alpha_0$ describes a uniform circular motion with cyclotron frequency $\omega_0 = eB_0/(mc)$ and radius $R = v_F/\omega_0$. This is obviously correct in the absence of modulation fields, where the position of the GC $\mathbf{r}_{\text{gc}}(t)$ is a constant of motion, and in the presence of a homogeneous in-plane electric field $\mathbf{E} \perp \mathbf{B}_0$, where the GC moves with the constant drift velocity $\dot{\mathbf{r}}_{\text{gc}} = c(\mathbf{E} \times \mathbf{B}_0)/B_0^2$. For a perturbation by a position-dependent in-plane electric field $\mathbf{E} = \nabla V(\mathbf{r})/e$ or perpendicular magnetic field $\mathbf{B}_m = (0, 0, B_m(\mathbf{r}))$, the GC picture is only approximately valid, and several definitions of a “guiding center” are possible, which become equivalent in the limit of small perturbations.

A reasonable candidate is the center of the circle of curvature at the point $\mathbf{r}(t)$. Taking the energy conservation $(m/2)v^2 + V(\mathbf{r}) = E_F$ into account and writing the velocity as $\dot{\mathbf{r}} = \mathbf{v} = v(\mathbf{r})(\cos \varphi, \sin \varphi, 0)$ with $v(\mathbf{r}) = v_F[1 - V(\mathbf{r})/E_F]^{1/2}$, this center is given by¹⁶

$$\mathbf{r}_M = \mathbf{r} + \mathbf{e}_z \times \mathbf{v}/(\omega_0 + \omega_{\text{mod}}), \quad (2)$$

where $\omega_{\text{mod}} = \omega_m + [\mathbf{e}_z \times (\mathbf{v}/v)] \cdot \nabla v(\mathbf{r})$ with $\omega_m(\mathbf{r}) = eB_m(\mathbf{r})/(mc)$.

To lowest order in the modulation strength one may neglect the modulation effect ω_{mod} in the denominator of Eq. (2). Then Newton’s equation $m\dot{\mathbf{v}} = -e[\mathbf{E} + (\mathbf{v}/c) \times (\mathbf{B}_0 + \mathbf{B}_m)]$ yields the time derivatives¹⁶

$$\dot{x}_M = c \frac{E_y}{B_0} - v_x \frac{\omega_m}{\omega_0}, \quad \dot{y}_M = -c \frac{E_x}{B_0} - v_y \frac{\omega_m}{\omega_0}. \quad (3)$$

In the spirit of the GC picture we may average Eq. (3) over the rapid cyclotron motion, i.e., we approximate $\mathbf{v} \approx$

$\dot{\mathbf{r}}_{\text{cyc}}$, replace $\mathbf{r}(t) = \mathbf{r}_{\text{gc}}(t) + \mathbf{r}_{\text{cyc}}(t)$ in the arguments of \mathbf{E} and ω_m , and take the average with respect to $\alpha = \omega_0 t$ over one period. We assume that $V(\mathbf{r})$ and $\omega_m(\mathbf{r})$ are periodic, with vanishing average values, on the same rectangular lattice with lattice constants $a_x = 2\pi/K_x$ and $a_y = 2\pi/K_y$,

$$V(\mathbf{r}) = \sum_{\mathbf{q} \neq \mathbf{0}} V_{\mathbf{q}} e^{i\mathbf{q} \cdot \mathbf{r}}, \quad \omega_m(\mathbf{r}) = \sum_{\mathbf{q} \neq \mathbf{0}} \omega_{\mathbf{q}} e^{i\mathbf{q} \cdot \mathbf{r}}, \quad (4)$$

where $\mathbf{q} = (n_x K_x, n_y K_y)$. The averages over the cyclotron motion can be performed for each Fourier component separately.¹⁶ The result of this approximation is the equation of motion for the GC,

$$\dot{\mathbf{r}}_{\text{gc}} = \mathbf{v}_{\text{gc}} = -\frac{1}{m\omega_0} \mathbf{e}_z \times \nabla V_{\text{eff}}(\mathbf{r}_{\text{gc}}), \quad (5)$$

where the effective potential $V_{\text{eff}}(\mathbf{r}) = \sum_{\mathbf{q} \neq \mathbf{0}} e^{i\mathbf{q} \cdot \mathbf{r}} V_{\mathbf{q}}^{\text{eff}}$, is determined by^{16,18}

$$V_{\mathbf{q}}^{\text{eff}} = V_{\mathbf{q}} J_0(qR) + \frac{mv_F}{q} \omega_{\mathbf{q}} J_1(qR), \quad (6)$$

with Bessel functions J_0 and J_1 . According to Eq. (5), the GC moves along the equipotential lines of the effective potential $V_{\text{eff}}(\mathbf{r}_{\text{gc}})$. Note that, in Eq. (5), we have identified the GC with the average value (over one cyclotron cycle) of $\mathbf{r}_M(t)$ as defined in Eq. (2), and that we have taken into account only terms in lowest order of $\omega_{\text{mod}}/\omega_0 \ll 1$.

B. Examples and limitations

We have, for a large number of examples, integrated Newton’s equation numerically to obtain the exact trajectories $\mathbf{r}(t)$ and $\mathbf{r}_M(t)$ as defined in Eq. (2), and also with the approximation $\omega_{\text{mod}}/\omega_0 \rightarrow 0$. We found that in all cases with sufficiently small modulations (roughly $|\omega_{\text{mod}}| \lesssim 0.2\omega_0$) the average of $\mathbf{r}_M(t)$ and of its approximation for $\omega_{\text{mod}} \rightarrow 0$ are practically identical. Moreover, these averages agree with the average of the exact trajectory $\mathbf{r}(t)$ over the cyclotron motion, which we have calculated as

$$\bar{\mathbf{r}}(t) = \frac{1}{T_+(t) - T_-(t)} \int_{T_-(t)}^{T_+(t)} dt' \mathbf{r}(t'), \quad (7)$$

where $\varphi(T_{\pm}) = \varphi(t) \pm \pi$, and $\varphi(t)$ defines the direction of the velocity at time t , $\dot{\mathbf{r}}(t) = v(\mathbf{r}(t))(\cos \varphi(t), \sin \varphi(t), 0)$. This rather complicated definition of the time average seems necessary, since in the 2D LSL the velocity vector $\dot{\mathbf{r}}(t)$ is not an exactly periodic function of time, in contrast to the case of drifting orbits in a 1D LSL.¹³

As a typical example we show in Fig. 1, for two different modulation strengths of a square-symmetric electrical modulation, rosette-like orbits together with $\mathbf{r}_M(t)$ (in the limit $\omega_{\text{mod}} \rightarrow 0$) and $\bar{\mathbf{r}}(t)$ defined by Eqs. (2)

and (7), respectively. For weak modulation, both definitions yield trajectories close to equipotentials, as expected from Eq. (5). However, $\mathbf{r}_M(t)$ exhibits rapid fluctuations around its equipotential, with an amplitude that increases with the modulation strength. Using the cyclotron motion as a reference, we see from Fig. 1 that the velocity of the GC motion increases (essentially linearly) with increasing modulation strength.

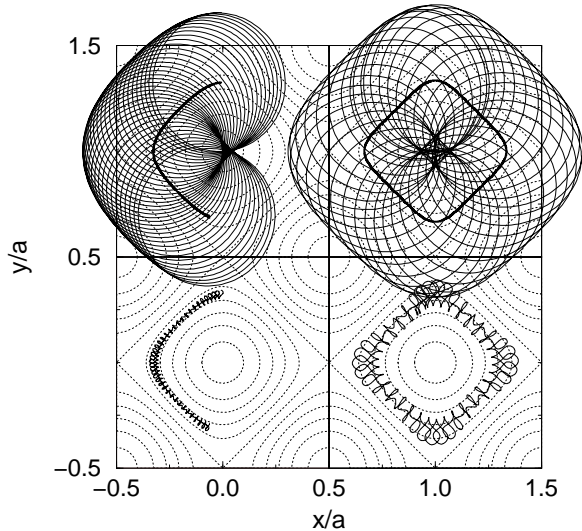


FIG. 1. Parts of rosette-like orbits (about 39 cyclotron cycles, same initial conditions) in the electric modulation potential $V(x, y) = \varepsilon E_F[\cos qx + \cos qy]$, with $q = 2\pi/a$ and $qR = 2$, for $\varepsilon = 0.05$ (left) and $\varepsilon = 0.15$ (right). Thick solid lines show the corresponding $\bar{\mathbf{r}}(t)$ as defined by Eq. (7), thin dotted lines the equipotentials of $V(x, y)$. The corresponding $\mathbf{r}_M(t)$, Eq. (2) with $\omega_{\text{mod}} = 0$, are shifted downwards by one lattice period.

If the modulation has only a rectangular instead of a square symmetry, the GCs may follow either closed (localized) or open (drifting) equipotentials. A typical example with an electrostatically defined LSL is shown in Fig. 2.

We want to mention that there are situations in which the GC picture works, but Eq. (5) does not. This is, e.g., the case, if due to the Bessel functions in Eq. (6) the effective potential vanishes for finite modulation, and therefore the first order approximation Eq. (5) fails. For the square-symmetric harmonic electric modulation considered in Fig. 1, this happens for $J_0(qR) = 0$ (“electric flat-band condition”). Then, besides orbits with GCs moving around potential maxima [$\mathbf{r} = (ma, na)$] and minima [$\mathbf{r} = (2m + 1, 2n + 1)a/2$], there are also orbits with GCs moving around saddle points at [$\mathbf{r} = (2m, 2n + 1)a/2$] and [$\mathbf{r} = (2m + 1, 2n)a/2$], which are not described by Eq. (5). The approximation Eq. (5) becomes also poorer with increasing modulation strength. Thus, we see from the right thick line in Fig. 1 that the GC deviates char-

acteristically from the equipotential trajectory predicted by Eq. (5).

The failure of Eq. (5) near the “flat-band conditions” is not very important for the calculation of the conductivity, since there the GC drift is anyway slow and thus contributes little to the conductivity. There are, however, natural limitations of the GC picture. Of course, if the (average) magnetic field B_0 becomes too strong, the classical approach fails and Landau quantization effects must be taken into account. If B_0 is zero or very small, “channeled orbits” occur similar to the case of a 1D LSL.¹³ In contrast to the 1D case, in 2D LSL one also observes chaotic orbits^{20,21} if the modulation is sufficiently strong and B_0 is sufficiently small, $\omega_{\text{mod}} \gtrsim \omega_0$. In the regime of chaotic orbits (i.e., for the model of Fig. 1 with $\varepsilon \sim 0.05$ for $qR \gtrsim 7$) the GC picture is not useful, since it does not simplify the description of the electron motion.

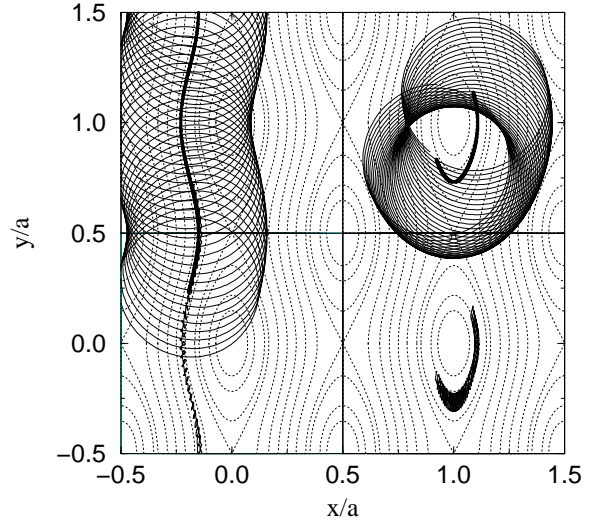


FIG. 2. Thirty-eight cyclotron cycles of a drifting (left) and of a localized (right) orbit in the electric modulation potential $V(x, y) = 0.1 E_F[\cos qx + 0.25 \cos qy]$ (equipotentials indicated by thin dotted lines), with $q = 2\pi/a$ and $qR = 2$. Thick solid lines: GC trajectories as defined by Eq. (7). The rapidly fluctuating trajectories of $\mathbf{r}_M(t)$, Eq. (2) with $\omega_{\text{mod}} = 0$, are shifted downwards by one period.

In the following we will consider the decomposition of Eq. (1) for the electron motion in a LSL and calculate the GC motion from Eq. (5). This is a good approximation if the modulation fields defining the LSL are sufficiently weak and if the average magnetic field B_0 is sufficiently strong. We want to emphasize that the GC picture yields reasonable results for the magnetoconductivity even in situations in which Eq. (1) with $\mathbf{r}_{\text{gc}}(t)$ calculated from Eq. (5) does not yield a reasonable approximation for an individual trajectory $\mathbf{r}(t)$ with the same initial conditions.

C. Conductivity from GC motion

To calculate the magnetoconductivity of a 2D EG in a LSL within the relaxation time approximation, we use Einstein's relation $\sigma_{\mu\nu} = D_{\mu\nu} e^2 m / (\pi \hbar^2)$ and the Chambers formula^{22,16} for the diffusion tensor $D_{\mu\nu}$, which contains the velocity autocorrelation integral along a trajectory, averaged over all initial conditions $\mathbf{r}(0) = \mathbf{r}_0$, $\dot{\mathbf{r}}(0) = v(\mathbf{r}_0)(\cos \varphi_0, \sin \varphi_0)$. With the decomposition of Eq. (1) this yields three types of terms. One term, which contains only the cyclotron velocity and must be averaged over the initial value α_0 , yields the Drude conductivity tensor. The mixed terms, containing both the cyclotron and the GC velocity, vanish upon averaging over α_0 . Finally, the term containing only the GC drift contribution is given by

$$D_{\mu\nu}^{\text{gc}} = \int_0^\infty dt e^{-t/\tau} \left\langle v_\mu^{\text{gc}}(t) v_\nu^{\text{gc}}(0) \right\rangle_{\text{init}}, \quad (8)$$

where the average has to be taken over all possible initial positions $\mathbf{r}_{\text{gc}}(0)$ of GC trajectories in a unit cell of the periodic potential.

With the dimensionless coordinates $\xi = K_x x$ and $\eta = K_y y$ and the effective potential

$$w(\xi, \eta) = \sum_{m,n} e^{i(m\xi + n\eta)} V_{(mK_x, nK_y)}^{\text{eff}} / V_{\text{cha}}, \quad (9)$$

where V_{cha} is an energy characteristic for $V_{\text{eff}}(\mathbf{r})$, e.g. its maximum, Eq. (5) reads

$$\frac{d\xi}{dt} = \Omega \frac{\partial w}{\partial \eta}, \quad \frac{d\eta}{dt} = -\Omega \frac{\partial w}{\partial \xi}, \quad (10)$$

with

$$\Omega = K_x K_y \frac{V_{\text{cha}}}{m\omega_0}. \quad (11)$$

Given the analytical form of the effective potential $w(\xi, \eta)$, we can use Eqs. (10) to calculate the diffusion tensor (8) as an integral over the equipotentials of $w(\xi, \eta)$ (see appendix A). The results then depend only on the parameter $\Omega\tau$. In the following section we will demonstrate this with a few explicit examples.

III. RESULTS AND EXAMPLES

To keep the notation simple, we will in the following consider only superlattices with a rectangular symmetry, with 1D and square-symmetric LSL as limiting cases.

A. One-dimensional modulation

If the periodic potential depends only on one coordinate, say $w(\xi)$, Eq. (10) yields $v_x = \dot{\xi}/K_x = 0$,

$\xi(t) = \xi(0)$, and $v_y = w'(\xi(0))/K_y$, independent of time. Thus we can immediately evaluate Eq. (8) to obtain $D_{xx}^{\text{gc}} = D_{xy}^{\text{gc}} = D_{yx}^{\text{gc}} = 0$ and

$$D_{yy}^{\text{gc}} = \frac{\Omega^2 \tau}{K_y^2} \int_{-\pi}^{\pi} \frac{d\xi}{2\pi} [w'(\xi)]^2 \equiv \tau \left[\frac{K_x V_{\text{cha}}}{m\omega_0} \right]^2 \left\langle [w'(\xi)]^2 \right\rangle_{\xi}. \quad (12)$$

For simple harmonic modulations, e.g., $V_{\mathbf{q}} = \delta_{\mathbf{q},(\pm K,0)} V_K$ and $\omega_{\mathbf{q}} = \delta_{\mathbf{q},(\pm K,0)} \omega_{\pm K}$ with $\omega_{-K} = \omega_K^*$ in Eq. (4), one obtains from Eq. (6) $V_{\text{eff}}(\mathbf{r}) = \tilde{V}_0 \cos(Kx + \alpha)$, with $\tilde{V}_0 = 2|V_{(K,0)}^{\text{eff}}|$. With $V_{\text{cha}} = \tilde{V}_0$ and $w'(\xi) = -\sin(\xi + \alpha)$, Eq. (12) reproduces the known formula¹⁶

$$\Delta\sigma_{yy}^{\text{1D}} = \frac{e^2 m}{\pi \hbar^2} \frac{\Omega^2 \tau}{2K^2}, \quad (13)$$

where the WO result from the oscillatory behavior of

$$\Omega = \frac{K^2 v_F^2}{\omega_0} \left| \frac{V_K}{E_F} J_0(KR) + \frac{2\omega_K}{K v_F} J_1(KR) \right|. \quad (14)$$

Here a complex ratio ω_K/V_K allows to describe a phase-shift between electric and magnetic modulation.

B. Weak 2D modulation, $\Omega\tau \ll 1$

For a 2D superlattice potential one obtains a similar simple result, if the modulation amplitude (or the relaxation time τ) is sufficiently small, so that $\Omega\tau \ll 1$. Then we may approximate $v_\mu(t) \approx v_\mu(0)$ in Eq. (8), so that the t integral becomes trivial, with the result

$$D_{\mu\nu}^{\text{gc}} = \frac{\sigma_\mu \sigma_\nu}{K_\mu K_\nu} \frac{\Omega^2 \tau}{(2\pi)^2} \int_{-\pi}^{\pi} d\xi \int_{-\pi}^{\pi} d\eta w_{\bar{\mu}} w_{\bar{\nu}} \quad (15)$$

with $\sigma_x = 1$, $\sigma_y = -1$, $w_x = \partial w / \partial \xi$, $w_y = \partial w / \partial \eta$ and the notation $\bar{\mu} = y$ (or x) if $\mu = x$ (or y). The factor $(2\pi)^2$ is the area of the dimensionless unit cell.

If the periodic potential is additive, $w(\xi, \eta) = w^{(1)}(\xi) + w^{(2)}(\eta)$, the off-diagonal elements vanish, $D_{xy}^{\text{gc}} = D_{yx}^{\text{gc}} = 0$, and the diagonal elements agree with those of the corresponding 1D modulations, Eq. (12).

This weak-modulation limit $\Omega\tau \ll 1$, in which the magnetoconductivity is independent of the nature of the GC trajectories, has been discussed in Ref.¹⁶. However, with increasing modulation strength (and larger relaxation time, i.e. larger mean free path) the nature of the GC trajectories will become important. For $\Omega\tau \gg 1$ the time integral will be proportional to the average velocity along the trajectory. For closed trajectories, this average will vanish, whereas for open equipotentials, which may exist either in x or in y direction, the average may be finite. Thus we expect that, in the limit $\Omega\tau \rightarrow \infty$, closed equipotentials will not contribute to the diffusion tensor, whereas the contribution of open ones will be similar to the case of 1D modulation.

C. Square-symmetric harmonic modulation

We now consider the 2D version of the simple harmonic modulation discussed in Sect. III A, i.e., assume in Eq. (4) $V_{\mathbf{q}} = (\delta_{\mathbf{q},(\pm K,0)} + \delta_{\mathbf{q},(0,\pm K)})V_K$ and $\omega_{\mathbf{q}} = (\delta_{\mathbf{q},(\pm K,0)} + \delta_{\mathbf{q},(0,\pm K)})\omega_{\pm K}$ with $\omega_{-K} = \omega_K^*$. Then the effective potential has the form

$$V_{\text{eff}}(\mathbf{r}) = \tilde{V}_0[\cos(Kx + \alpha) + \cos(Ky + \alpha)], \quad (16)$$

with an (irrelevant) phase shift α , and all equipotentials are closed lines around either a maximum or a minimum, except those for $V_{\text{eff}}(\mathbf{r}) = 0$, which are straight lines. We find that the angular velocity of the GC drift along the equipotentials is given only by the parameter Ω defined in Eq. (14), and geometrical factors. As a consequence, the suppression of the GC contribution to the conductivity can be expressed by a function $\Phi(\Omega\tau)$, and instead of Eq. (13) we obtain

$$\sigma_{xx}^{2D} = \sigma_{yy}^{2D} = \frac{e^2 m \Omega^2 \tau}{\pi \hbar^2 2K^2} \Phi(\Omega\tau), \quad (17)$$

and $\sigma_{xy}^{2D} = \sigma_{yx}^{2D} = 0$. The actual calculation of $\Phi(\Omega\tau)$ is sketched in Appendix A. The numerical results are plotted as diamonds in Fig. 3, together with some analytical approximations, which are obtained from the asymptotic behavior of the correct result for small and large values of $\Omega\tau$ (see Appendix B). Apparently the three-parameter interpolation formula

$$\Phi_3(\Omega\tau) = [1 + 0.25(\Omega\tau)^2] / [1 + 0.75(\Omega\tau)^2 + 0.076(\Omega\tau)^4] \quad (18)$$

provides a very good fit to the correct numerical result for all values of $\Omega\tau$. Note that $\Phi(\Omega\tau) \rightarrow 1$ for $\Omega\tau \rightarrow 0$, as we expect for the weak-modulation limit.

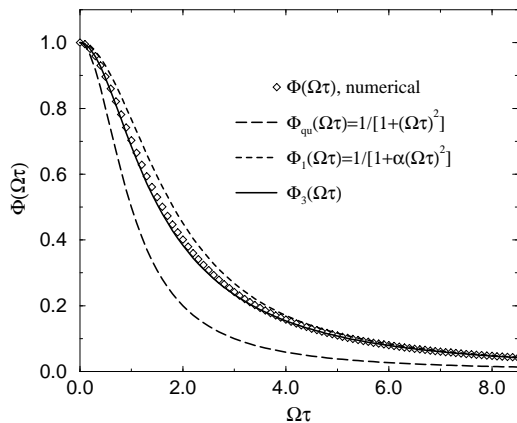


FIG. 3. Suppression of conductivity in 2D superlattice with square symmetry; numerical result $\Phi(\Omega\tau)$ (open diamonds), quadratic approximation with cut-off energy $\epsilon_{\text{qu}} = 0.228$ (long-dashed), one-parameter interpolation with $\alpha = 0.304$ (dashed), and the three-parameter interpolation of Eq. (18) (solid line).

We want to emphasize that, for the square-symmetric harmonic cosine modulation the suppression of the GC induced contribution to the conductivity is described by the single parameter $\Omega\tau$ which, according to Eq. (14), itself depends on modulation strength and period, and on the cyclotron radius $R = v_F/\omega_0$.

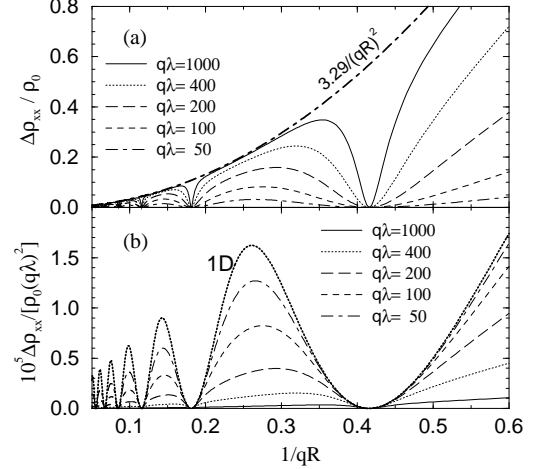


FIG. 4. (a) GC drift contribution to the conductivity versus magnetic field in units $1/qR$ for electric modulation $V(x, y) = 0.02E_F[\cos qx + \cos qy]$ and several values of the mean free path between $q\lambda = 50$ (lower dash-dotted) and 1000 (upper solid line). (b) Same resistance data divided by $(q\lambda)^2$, compared with result for the one-dimensional modulation $V(x) = 0.02E_F \cos qx$ (thick line) which is independent of $q\lambda$.

As an instructive example, we plot in Fig. 4(a), under the assumption $\omega_0\tau \gg 1$, the GC contribution $\Delta\rho_{xx}/\rho_0 \approx (\omega_0\tau)^2 \Delta\sigma_{yy}/\sigma_0$ for the electric modulation $V(x, y) = 0.02E_F[\cos qx + \cos qy]$ and several values of the mean free path $\lambda = v_F\tau$ ($\sigma_0 = 1/\rho_0 = e^2 n_{e1}\tau/m$). Away from the flat band conditions, given here by the zeroes of the Bessel function J_0 , $\Omega\tau$ becomes large with large mean free path, and $\Delta\rho_{xx}/\rho_0 \approx (\Omega\tau)^2 \Phi(\Omega\tau)/(qR)^2$ approaches the limiting curve $3.29/(qR)^2$, which is also indicated in Fig. 4(a). We see that, as compared with the Drude resistance ρ_0 of the homogeneous system, the modulation induced correction to the resistance increases with increasing mean free path and finally saturates. Since the shape of the resistivity curves in Fig. 4 depends only on the parameter $\Omega\tau$ and Ω is proportional to the modulation strength, variation of the modulation strength leads to a set of curves similar to that shown in Fig. 4(a) for the variation of $(q\lambda)^2$. With increasing modulation strength the curves will saturate and approach the same limiting curve, indicated as thick dash-dotted line in Fig. 4(a).

On the other hand, if we compare this modulation correction calculated for the square symmetric case with that obtained for the corresponding 1D modulation, we find, with increasing mean free path, an increasingly

strong suppression of the WO. This becomes evident from Fig. 4(b), where we have divided $\Delta\rho_{xx}/\rho_0$ by $(q\lambda)^2$, since with this normalization the 1D result becomes independent of $q\lambda$. In this plot the suppression of the resistivity maxima becomes stronger with increasing mean free path and increasing modulation strength.

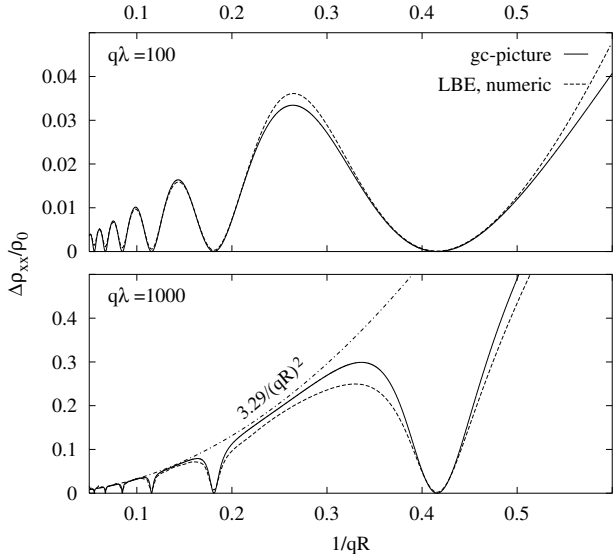


FIG. 5. Comparison of resistivities calculated for electric modulation $V(x, y) = 0.02E_F[\cos qx + \cos qy]$ within the GC picture (solid lines) and from numerical solution of the linearized Boltzmann equation (dotted lines), for two values of the mean free path.

To show that the GC picture yields reasonable results, we compare in Fig. 5 calculations based on Eqs. (17) and (18) with results obtained numerically from the linearized Boltzmann equation. The Boltzmann equation was solved by Fourier expansion of the distribution function with respect to the periodic position variables x and y and the angle φ in velocity space, similar to the procedure described in Ref.¹⁵ for a 1D LSL. To obtain the curve for $q\lambda = 1000$ with sufficient accuracy, about 40 000 Fourier coefficients had to be included, and the calculation, using an optimized parallel code, took about 6 hours on a CRAY-T3E with 128 nodes. The comparison shows that the GC approach with the approximation (18), which requires only negligible numerics, yields surprisingly good results for weak modulations. The agreement will become poorer for stronger modulation and for much smaller $q\lambda$. Then, with decreasing B_0 , the maxima of the $\Delta\rho_{xx}$ oscillations in the GC approach will still extrapolate to zero, whereas the correct calculation yields damped oscillations around a nearly constant, finite $\Delta\rho_{xx}$ value. But this difference occurs also for 1D LSLs and is well understood.¹⁵

We conclude that the GC approach yields reasonable results for not too strong modulations (and not too small $q\lambda$ values), and we will use it as a versatile approach to discuss interesting situations of lower symmetry.

Pure magnetic modulations lead to similar results as pure electric modulations, of course with modifications due to the differences between the Bessel functions J_1 and J_0 , notably a phase shift. Interesting new situations occur for mixed electric and magnetic modulations, which can be achieved experimentally, e.g., by bringing a rectangular pattern of ferromagnetic islands on the surface of the sample.²³ Superpositions of harmonic electric and magnetic modulations, eventually with a phase shift, can easily be evaluated using Eq. (18), provided the effective potential according to Eq. (6) has square symmetry.

D. Harmonic LSL with rectangular symmetry

A LSL with exact square-symmetry is an idealized limiting case and hard to realize experimentally. Therefore, we now consider the more general case of a rectangular LSL, which allows to interpolate between 1D and square-symmetric 2D modulations, and to approach both limiting cases. To keep the discussion simple, we restrict it on harmonic electric and magnetic modulations in both directions, so that the effective potential is of the form

$$V_{\text{eff}}(\mathbf{r}) = \tilde{V}_x \cos(K_x x + \alpha_x) + \tilde{V}_y \cos(K_y y + \alpha_y), \quad (19)$$

where the ratios of amplitudes and phases may depend on the amplitudes and relative phases between the electric and magnetic modulations in x and in y direction, and, in contrast to Eq. (16), on the average magnetic field B_0 .

Besides its simplicity, this model is important for the physical reason, that higher modulation harmonics decrease exponentially with the distance of the 2D EG from the surface if the modulation is produced by some type of surface structuring. Thus, if this distance is large enough, it will be sufficient to consider only the basic cosine modulation.

1. Numerical and analytical results

For a given modulation, the ratio \tilde{V}_y/\tilde{V}_x in Eq. (19) may change magnitude and sign as a function of B_0 . This can lead to interesting switching effects which we will discuss below. For the calculation of the conductivity components (Appendix A), we assume however always $0 \leq \kappa = \tilde{V}_y/\tilde{V}_x \leq 1$, which may eventually require an interchanging of x and y in the final results. Then, with $V_{\text{cha}} = \tilde{V}_x$ in Eqs. (9) and (11), and with a suitable choice of the origin, the dimensionless potential (9) becomes

$$w(\xi, \eta) = \cos \xi + \kappa \cos \eta, \quad 0 \leq \kappa \leq 1. \quad (20)$$

For $\kappa = 0$ we have the 1D modulation in x direction, and the equipotentials are straight lines in y direction. For $\kappa = 1$ we have the square-symmetric case where all equipotentials are closed lines. These cases have been considered above. For $0 < \kappa < 1$, there exist closed

equipotentials with $w(\xi, \eta) = \epsilon$ around maxima in the energy interval $1 - \kappa < \epsilon \leq 1 + \kappa$, closed equipotentials around minima in the interval $-(1 + \kappa) \leq \epsilon < -(1 - \kappa)$, and open equipotentials in y direction for $-(1 - \kappa) \leq \epsilon \leq 1 - \kappa$. We can show that, in the limit of large mean free path ($\tau \rightarrow \infty$), the GC contribution $\Delta\sigma_{xx}$ comes only from closed orbits, and shows a suppression similar to that obtained in the square-symmetric case. The contributions to $\Delta\sigma_{yy}$, on the other hand, come from both closed and open equipotentials. The latter lead to an increase with increasing τ , similar to the 1D case.

The off-diagonal components $\Delta\sigma_{xy} = \Delta\sigma_{yx} = 0$ can be shown to vanish from symmetry reasons. The analytical considerations of Appendix A show that the diagonal components can be written as

$$\Delta\sigma_{\mu\mu} = \frac{e^2 m}{\pi \hbar^2} \frac{\Omega^2 \tau}{2K_\mu^2} \Phi_{\mu\mu}(\Omega\tau, \kappa), \quad (21)$$

with $\Omega = K_x K_y \tilde{V}_x / (m\omega_0)$, so that the (suppression) effect of the 2D modulation now is described by two parameters, $\Omega\tau$ and κ . We have numerically calculated the functions $\Phi_{\mu\mu}(\Omega\tau, \kappa)$, which of course satisfy the consistency relations $\Phi_{xx}(\Omega\tau, 1) \equiv \Phi_{yy}(\Omega\tau, 1) \equiv \Phi(\Omega\tau)$. Since it is rather time-consuming to calculate the successive fourfold integrals with sufficient accuracy for each specific example anew, we tried to fit the $\Phi_{\mu\mu}(\Omega\tau, \kappa)$ by simple analytic expressions. We found that the numerical results for $\Phi_{xx}(\Omega\tau, \kappa)$ are very well (with an error of less than 1 per cent) approximated by $\kappa^2 \Phi(\Omega\tau)$, so that a good approximation is

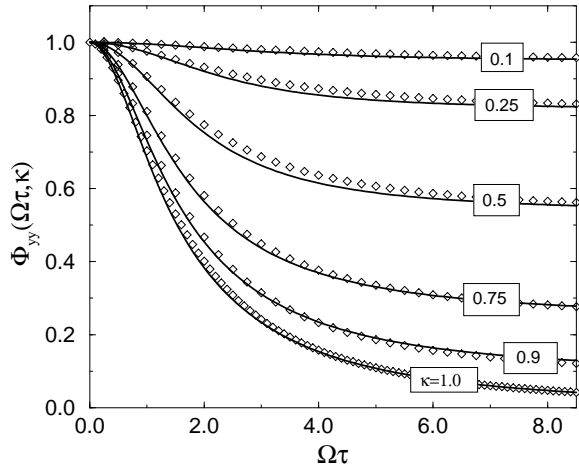


FIG. 6. Numerical result for $\Phi_{yy}(\Omega\tau, \kappa)$ (diamonds) for several values of the anisotropy parameter $\kappa = \tilde{V}_y/\tilde{V}_x$. The solid lines are for the approximation $\Phi_{yy}^{(3)}$, Eq. (24).

$$\Phi_{xx}(\Omega\tau, \kappa) \approx \kappa^2 \Phi(\Omega\tau) \approx \kappa^2 \Phi_3(\Omega\tau), \quad (22)$$

with $\Phi_3(\Omega\tau)$ defined by Eq. (18). Numerical results for $\Phi_{yy}(\Omega\tau, \kappa)$ are shown as diamonds in Fig. 6. Apparently, for $\kappa < 1$ they approach a finite limit for $\Omega\tau \rightarrow \infty$. This

limit $\Phi_{yy}(\infty, \kappa)$ is easily calculated numerically and well approximated by

$$\Phi_2(\kappa) = 1 - 1.645 \kappa^{3/2} + 0.645 \kappa^{5/2}, \quad (23)$$

see Appendix B. Incorporating this into an interpolation formula that reduces for $\kappa = 1$ to the previous fit (18), we obtained

$$\Phi_{yy}^{(3)}(\Omega\tau, \kappa) = \Phi_2(\kappa) + \frac{[1 - \Phi_2(\kappa)][1 + \alpha_\kappa (\Omega\tau)^2]}{1 + (\alpha_\kappa + \beta_\kappa) (\Omega\tau)^2 + \gamma_\kappa (\Omega\tau)^4}, \quad (24)$$

with $\alpha_\kappa = 0.25 \sin^2(\pi\kappa/2)$, $\beta_\kappa = 0.5\kappa^2/[1 - \Phi_2(\kappa)]$, and $\gamma_\kappa = 0.076 \sin^2(\pi\kappa/2)$. This approximation is indicated by the lines in Fig. 6 and will in the following be used instead of $\Phi_{yy}(\Omega\tau, \kappa)$.

2. Two examples

First we consider in Fig. 7 a purely electrostatic modulation on a square lattice, $a_x = a_y = 2\pi/q$, $V(x, y) = V_x \cos(qx) + V_y \cos(qy)$, so that $\tilde{V}_\mu = V_\mu |J_0(qR)|$ and the ratio $\kappa = \tilde{V}_y/\tilde{V}_x = V_y/V_x$ is independent of B_0 , and $\Omega = q^2 V_x |J_0(qR)| / (m\omega_0)$.

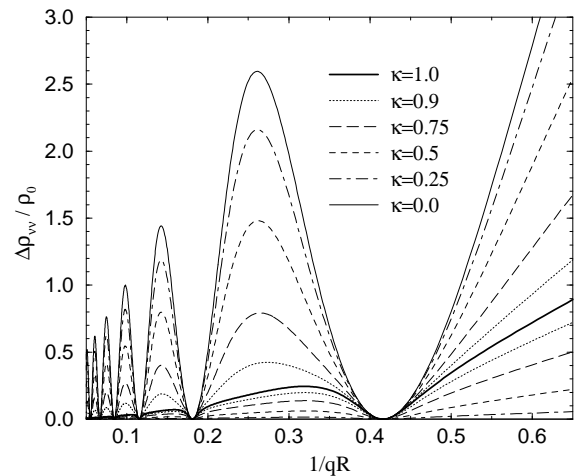


FIG. 7. GC contribution to the resistivities for the electrostatic modulation $V(x, y)/E_F = 0.02 [\cos(qx) + \kappa \cos(qy)]$ and $q\lambda = 400$. For $\kappa = 1$ (thick line) $\Delta\rho_{xx} = \Delta\rho_{yy}$. For $\kappa < 1$, the result for $\Delta\rho_{yy}$ lies below, that for $\Delta\rho_{xx}$ above this thick line, and both are indicated by the same line style.

For $\kappa < 1$, there exist open equipotentials only in y direction. With decreasing κ their number increases, and $\Delta\rho_{xx}$ increases towards the results for the 1D modulation ($\kappa = 0$). Simultaneously $\Delta\rho_{yy} \propto \kappa^2$ decreases, and vanishes in the 1D limit. The degree of anisotropy increases with both the modulation amplitude and the mean free

path, since, for $\Omega\tau \gg 1$, $\Delta\rho_{yy}/\rho_0 \approx 3.29\kappa^2/(qR)^2$ saturates, while $\Delta\rho_{xx}/\rho_0 \sim (\Omega\tau)^2\Phi_2(\kappa)/(qR)^2$ increases without limit.

The anisotropy parameter κ is only a constant independent of B_0 if we have either a pure electric or a pure magnetic modulation on a square lattice, i.e., with the same period in x and y direction. In all other situations, the Bessel functions in Eq. (6) lead to a B_0 -dependent κ . In such cases we use the following convention to express the relevant parameters Ω and κ in terms of the original parameters specifying the modulation.

We measure energies in units of $E_F = mv_F^2/2$ and the average magnetic field in dimensionless units $1/(qR)$, where $R = v_F/\omega_0$ is the cyclotron radius and $q = \sqrt{K_x K_y}$. Then, for a suitable choice of the coordinate system, the modulation may depend on the following seven parameters: (1) the ratio of the lattice constants $a_y/a_x = K_x/K_y$, (2) the amplitudes $\varepsilon_\nu = V_\nu/E_F$ of the electric cosine potential $V(x, y) = E_F[\varepsilon_x \cos(K_x x) + \varepsilon_y \cos(K_y y)]$, (3) the amplitudes $\mu_\nu = 2\omega_\nu/(K_\nu v_F)$ and (4) the relative phases α_ν of the effective magnetic modulation potential $E_F[\mu_x \cos(K_x x + \alpha_x) + \mu_y \cos(K_y y + \alpha_y)]$. For each value of the average magnetic field, we can calculate from these *seven* model parameters the *two* parameters of the effective potential (6) which are relevant for the conductivity, namely the absolute values of the complex numbers $\varepsilon_\nu J_0(K_\nu R) + \mu_\nu J_1(K_\nu R) \exp(i\alpha_\nu)$,

$$\tilde{\varepsilon}_\nu = \left\{ [\varepsilon_\nu J_0(K_\nu R) + \mu_\nu J_1(K_\nu R) \cos \alpha_\nu]^2 + [\mu_\nu J_1(K_\nu R) \sin \alpha_\nu]^2 \right\}^{1/2} \quad (25)$$

for $\nu = x, y$. The phases of these complex numbers can be compensated by a suitable shift of the coordinate system and have no effect on the conductivity. In the following we use these two parameters in the form $\varepsilon_{\max} = \max[\tilde{\varepsilon}_x, \tilde{\varepsilon}_y]$ and $\kappa = \min[\tilde{\varepsilon}_x, \tilde{\varepsilon}_y]/\max[\tilde{\varepsilon}_x, \tilde{\varepsilon}_y]$. Taking the characteristic energy in Eq. (11) as $V_{\text{cha}} = \varepsilon_{\max} E_F$, we obtain $\Omega = \omega_0 \varepsilon_{\max} (qR)^2/2$.

To characterize the system completely, we have to specify the mean free path $\lambda = v_F \tau$, which we write in the dimensionless form $q\lambda$, so that $\omega_0 \tau = \lambda/R$. Finally we obtain for the GC drift contribution to the conductivity tensor

$$\frac{\Delta\sigma_{\mu\mu}}{\sigma_0} = \frac{q^2}{4K_\mu^2} (qR\varepsilon_{\max})^2 \Phi_{\bar{\mu}\bar{\mu}} \left(\frac{1}{2} q^2 \lambda R \varepsilon_{\max}, \kappa \right), \quad (26)$$

with $\tilde{x} = y$ and $\tilde{y} = x$ if $\varepsilon_{\max} = \tilde{\varepsilon}_y$, and with $\tilde{x} = x$ and $\tilde{y} = y$ if $\varepsilon_{\max} = \tilde{\varepsilon}_x$. Since in the regime of commensurability oscillations $\omega_0 \tau \gg 1$, the GC correction to the resistivity tensor is $\Delta\rho_{\mu\mu}/\rho_0 = (\omega_0 \tau)^2 \Delta\sigma_{\bar{\mu}\bar{\mu}}/\sigma_0$, with $\bar{x} = y$ and $\bar{y} = x$.

As a very interesting example we consider a purely electrostatic modulation, but now on an rectangular superlattice with equal modulation amplitudes $\varepsilon_x = \varepsilon_y$ but different periods in both directions, $a_y/a_x = \sqrt{2}$. The interesting aspect of this model is that now the effective

potential changes its symmetry as a function of the magnetic field strength, since the arguments of the Bessel functions in Eq. (6) are different. If one of the Bessel functions vanishes, i.e. if the “flat-band” condition for this direction is satisfied, the effective potential shows a purely 1D modulation in the other direction. When the effective modulation potential in x direction is larger than that in y direction, there exist open equipotentials in y but not in x direction, and vice versa. Typical results for the resistivity corrections are shown in Fig. 8. For relatively small mean free path as in Fig. 8(a), the oscillations of the resistivity components $\Delta\rho_{\mu\mu}$ look similar to the results one would expect for the corresponding 1D modulations. At relatively low magnetic fields, there occurs however a kind of beating effect, manifested in a non-monotonous decrease of the oscillation amplitude of $\Delta\rho_{xx}$ (solid line) with decreasing magnetic field B_0 . The reason for this non-monotonous B_0 -dependence of the maxima is easily understood. The maxima occur nearly in the middle between adjacent flat-band conditions $J_0(K_x R) = 0$. If for these B_0 -values the effective modulation in y direction is large [i.e., if no zero of $J_0(K_y R)$ is close], the GC motion is essentially two-dimensional, and the maximum of $\Delta\rho_{xx}$ is suppressed below the corresponding one of a 1D modulation in x direction. If, however, the maximum of $\Delta\rho_{xx}$ appears near a zero of $J_0(K_y R)$, the modulation in y direction is small, and the $\Delta\rho_{xx}$ maximum assumes a large value close to that of the corresponding 1D modulation in x direction. This explains why the $\Delta\rho_{xx}$ maximum near $(qR)^{-1} = 0.071$ is higher than those near 0.091 and 0.116.

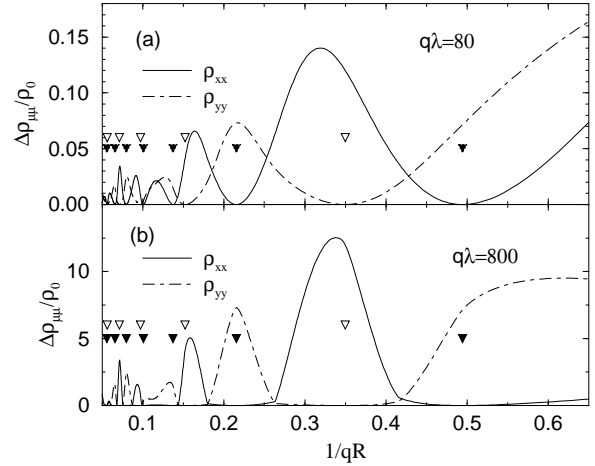


FIG. 8. GC contribution to the resistivities for modulation $V(x, y)/E_F = 0.02 [\cos(K_x x) + \cos(K_y y)]$, with $K_x/K_y = \sqrt{2}$, versus magnetic field in units of $1/qR$, with $q = \sqrt{K_x K_y}$; (a) for $q\lambda = 80$, (b) for $q\lambda = 800$. The “flat-band” conditions $J_0(K_x R) = 0$ and $J_0(K_y R) = 0$ are indicated by filled and open triangles, respectively.

These anisotropy effects are drastically enhanced for

larger mean free path, see Fig. 8(b). If, for example, at a given B_0 value the effective modulation potential in y direction is smaller than that in x direction, the contribution to $\Delta\rho_{yy}$ ($\propto \Delta\sigma_{xx}$) results only from guiding centers moving along closed equipotentials, and $\Delta\rho_{yy}/\rho_0$ is bounded by $3.29(\tilde{\varepsilon}_y/\tilde{\varepsilon}_x)^2/(qR)^2 \ll 3.29/(qR)^2$ (cf. Fig. 4). There exist, however, open equipotentials in y direction which lead to an increase of $\Delta\rho_{xx} \propto (q\lambda)^2$ with increasing mean free path. The result is a very effective switching as a function of the magnetic field B_0 between regions with large $\Delta\rho_{xx}$ and very small $\Delta\rho_{yy}$ and regions with small $\Delta\rho_{xx}$ and large $\Delta\rho_{yy}$, as is seen in Fig. 8(b).

If one mixes electric and magnetic modulations with different phase shifts in both directions, one may achieve such switching effects also on a square lattice, $K_x = K_y$.

IV. SUMMARY

We have evaluated the modulation correction to the magneto-resistivity tensor of 2D EGs in LSLs of rectangular symmetry within the GC picture. We have emphasized that this classical approach can be useful only within a restricted regime of sufficiently weak modulations and sufficiently strong (average) magnetic fields, where the electron motion may be approximated as a rapid cyclotron motion around slowly drifting GCs. Within this regime, in which a 2D EG with a 1D LSL exhibits regular commensurability oscillations (WO), we have investigated the effects of the model parameters (modulation strengths, anisotropy, phase shifts) and the mean free path on the amplitudes of the WO. For harmonic electro- and magnetostatic modulations we have obtained essentially analytical results.

The fact that the GCs move approximately along the equipotentials of a magnetic-field dependent effective potential, with a velocity essentially proportional to the strength of this potential, leads to an interesting dependence of the WO amplitudes on these model parameters. In contrast to a 1D LSL, which has only extended straight-line equipotentials, a 2D LSL has also closed equipotentials around the extrema of the effective potential. The difference between closed and extended equipotentials becomes important in the limit of a large mean free path, since the magnetoresistance is sensitive to the mean velocity of the GC motion between two successive scattering events. If the scattering time is sufficiently large, the GC velocity along closed equipotentials averages to zero, and then these equipotentials do not contribute to the magnetoresistance, whereas the contribution of extended equipotentials becomes very large.

This leads to strongly anisotropic resistivities, if the effective potential has rectangular but not square symmetry, and to very interesting magnetic-field dependent switching effects if the symmetry of the effective potential changes as a function of the average magnetic field.

For the 2D EG with a weak square-symmetric mod-

ulation we find with increasing mean free path an increasing suppression of the WO amplitudes below those obtained for the corresponding 1D modulation. This result provides a classical explanation of the suppression of the band-conductivity observed in early experiments on holographically modulated high-mobility samples,⁴ which previously has been explained with quantum arguments based on the subband splitting of the Hofstadter energy spectrum.^{6,11} For fixed mean free path, our (basically analytical) result reduces in the limit of very weak modulations to the predictions of Ref.¹⁶, without noticeable suppression of the WO. For realistic values of modulation strength and mean free path, our present results yield, however, a strong suppression. We want to point out that our present classical explanation of the WO suppression and the previous quantum one are not contradictory. Both need for the explanation of an effective suppression a sufficiently strong modulation and large mean free path (i.e. weak disorder).

Qualitatively our result is also in agreement with the recent prediction of the suppression of WO by Grant *et al.*¹⁸, which applies to the case of intermediate mean free path and strong 2D modulation. From our investigation of trajectories we expect, however, that for this strong modulation the regime of small and intermediate values of the average magnetic field is dominated by chaotic motion, so that the GC picture cannot be expected to yield quantitatively correct results.

Finally we want to comment on the fact that the Chambers formula (8) contains a scattering time, which describes isotropic impurity scattering, whereas calculations for the 2D EG with a 1D LSL based on Boltzmann's equation have revealed that predominantly small-angle impurity scattering has to be considered for a quantitative understanding of the WO amplitudes. We did not try to go beyond the simple relaxation time approximation in the GC picture, since (i) on the level of Boltzmann's equation, where we know how to describe anisotropic scattering, we cannot separate the GC from the cyclotron motion, and (ii) small-angle scattering of an electron between locally nearby trajectories may include large changes of the corresponding GCs, and we do not want to introduce unjustified assumptions on scattering between GCs. In view of the general limitations of the GC picture, we rather want to consider the relaxation time τ as a phenomenological parameter, which may be chosen to fit experiments qualitatively. We think, however, that τ should be considered as the total scattering time, which in the case of strongly anisotropic impurity scattering is much shorter than the transport or momentum relaxation time.

ACKNOWLEDGMENTS

We are grateful to J. H. Davies and A. R. Long for a stimulating discussion on the guiding-center picture

and to C. Albrecht for useful suggestions concerning the manuscript. This work was supported by BMBF Grant No. 01BM919/5.

APPENDIX A: CORRELATION INTEGRALS ALONG EQUIPOTENTIALS

To study the effect of closed equipotentials, we assume that the effective potential $w(\xi, \eta)$ has either isolated maxima or isolated minima, or both. For instance, the model (20) has, for arbitrary integers m and n , isolated maxima at $(\xi, \eta) = 2\pi(m, n)$ and isolated minima at $(\xi, \eta) = (2m + 1, 2n + 1)\pi$, and all equipotentials $w(\xi, \eta) = \epsilon$ for $|\epsilon| > 1 - \kappa$ are closed.

We assume that closed equipotentials around a maximum (minimum), which we take as origin, exist in the energy interval $\epsilon_{\max} \geq \epsilon > \epsilon_{\sup}$ ($\epsilon_{\min} \leq \epsilon < \epsilon_{\inf}$). In terms of polar coordinates,

$$\xi = \rho \cos \varphi, \quad \eta = \rho \sin \varphi, \quad -\pi < \varphi \leq \pi, \quad (\text{A1})$$

the equipotential with energy ϵ is described by the equation $\rho = \rho_\epsilon(\varphi)$, which maps φ onto the solution ρ of $w(\rho \cos \varphi, \rho \sin \varphi) = \epsilon$ for fixed ϵ and φ . Along the equipotential with energy ϵ the equations (10) reduce to

$$d\varphi/dt = \pm \Omega / \mathcal{J}_\epsilon(\varphi), \quad (\text{A2})$$

where the upper (lower) sign stands for orbits around a maximum (minimum), and

$$\mathcal{J}_\epsilon(\varphi) = \left| \frac{\rho_\epsilon(\varphi)}{\cos \varphi w_\xi + \sin \varphi w_\eta} \right|. \quad (\text{A3})$$

We can use Eq. (A2) to substitute in Eq. (8) the integration variable t by φ . Writing the initial position on an equipotential as $\mathbf{r}(0) = \rho_\epsilon(\varphi_0)(\cos \varphi_0, \sin \varphi_0)$, we get $t = \pm \int_{\varphi_0}^{\varphi} d\varphi' \mathcal{J}_\epsilon(\varphi') / \Omega$. With $2\theta_\epsilon = \int_{-\pi}^{\pi} d\varphi \mathcal{J}_\epsilon(\varphi)$ one obtains

$$\int_0^\infty dt e^{-t/\tau} w_\mu(\varphi(t); \epsilon) = \frac{\tau X W_\mu^\mp(\varphi_0, \varphi_0 \pm 2\pi; \epsilon)}{1 - e^{-2X\theta_\epsilon}}, \quad (\text{A4})$$

where $X = 1/(\tau\Omega)$ and

$$W_\mu^\pm(\varphi_0, \varphi_1; \epsilon) = \mp \int_{\varphi_0}^{\varphi_1} d\varphi \mathcal{J}_\epsilon(\varphi) w_\mu(\varphi; \epsilon) e^{\pm X \int_{\varphi_0}^{\varphi} d\varphi' \mathcal{J}_\epsilon(\varphi')}. \quad (\text{A5})$$

To evaluate the average over initial values in Eq. (8), we first integrate along the equipotentials with fixed energy ϵ and then over ϵ . It turns out that the Jacobian of the transformation from polar coordinates ρ, φ to the energy-angle coordinates ϵ, φ is just given by Eq. (A3), $d\rho d\varphi = d\epsilon d\varphi \mathcal{J}_\epsilon(\varphi)$. If the effective potential $w(\xi, \eta)$ is an even function of both arguments, we have $w_\mu(\varphi + \pi; \epsilon) = -w_\mu(\varphi; \epsilon)$ and $\mathcal{J}_\epsilon(\varphi + \pi) = \mathcal{J}_\epsilon(\varphi)$, and

all integrals over intervals of length 2π can be reduced to integrals over intervals of length π , and we obtain

$$D_{\mu\nu}^{\text{cl}, \pm} = \frac{\sigma_\mu \sigma_\nu}{K_\mu K_\nu} \frac{\Omega^2 \tau}{(2\pi)^2} \int_{a_\pm}^{b_\pm} d\epsilon \int_0^\pi d\varphi_0 \mathcal{J}_\epsilon(\varphi_0) \times w_{\bar{\nu}}(\varphi_0; \epsilon) \frac{2X W_{\bar{\mu}}^\mp(\varphi_0, \varphi_0 \pm \pi; \epsilon)}{1 + e^{-X\theta_\epsilon}} \quad (\text{A6})$$

with the upper sign and $a_+ = \epsilon_{\sup}$, $b_+ = \epsilon_{\max}$ for equipotentials around a maximum and the lower sign and $a_- = \epsilon_{\min}$, $b_- = \epsilon_{\inf}$ for those around a minimum.

Open equipotentials of a periodic potential with rectangular symmetry, by definition, connect one point on a boundary of the unit cell with the equivalent point on the opposite boundary. Since equipotential lines cannot cross each other, open equipotentials can exist either in x direction or in y direction, but not in both. Let us assume that in the energy interval $\epsilon_{\inf} \leq \epsilon \leq \epsilon_{\sup}$ open equipotentials in y direction exist. We may describe them in polar coordinates choosing the origin in a maximum, so that we can use the formalism developed above. Let the equipotential with energy ϵ hit the upper boundary of the unit cell at $\eta = \pi = \rho_\epsilon(\varphi_\epsilon) \sin \varphi_\epsilon$ for $\pi/4 \leq \varphi_\epsilon < \pi/2$. Assuming that $w(\xi, \eta)$ is even with respect to both arguments, we can show that the GC motion in negative y direction with initial conditions $\pi - \varphi_\epsilon \leq \varphi_0 \leq \pi + \varphi_\epsilon$ yields the same contribution to the diffusion tensor as those moving in the positive y direction with initial conditions $-\varphi_\epsilon \leq \varphi_0 \leq \varphi_\epsilon$, and we consider here only the latter.

For the time integration, we divide the infinite time interval into an initial one of duration $t_\epsilon = \Omega^{-1} \int_{\varphi_0}^{\varphi_\epsilon} d\varphi \mathcal{J}_\epsilon(\varphi)$ and subsequent intervals of duration $T_\epsilon = \Omega^{-1} \int_{-\varphi_\epsilon}^{\varphi_\epsilon} d\varphi \mathcal{J}_\epsilon(\varphi)$, which is the time a GC needs to traverse a unit cell on the equipotential of energy ϵ . Using the definition (A5), we obtain for the contribution of open orbits to the diffusion tensor

$$D_{\mu\nu}^{\text{open}} = \frac{\sigma_\mu \sigma_\nu}{K_\mu K_\nu} \frac{2X \Omega^2 \tau}{(2\pi)^2} \int_{\epsilon_{\inf}}^{\epsilon_{\sup}} d\epsilon \int_{-\varphi_\epsilon}^{\varphi_\epsilon} d\varphi_0 \mathcal{J}_\epsilon(\varphi_0) w_{\bar{\nu}}(\varphi_0; \epsilon) \times \left\{ W_{\bar{\mu}}^-(\varphi_0, \varphi_\epsilon; \epsilon) + \frac{e^{-t_\epsilon/\tau} W_{\bar{\mu}}^-(-\varphi_\epsilon, \varphi_\epsilon; \epsilon)}{1 - e^{-T_\epsilon/\tau}} \right\}. \quad (\text{A7})$$

To this we have to add the contribution of closed orbits according to Eq. (A6), $D_{\mu\nu}^{\text{gc}} = D_{\mu\nu}^{\text{open}} + D_{\mu\nu}^{\text{cl}, +} + D_{\mu\nu}^{\text{cl}, -}$. The result can be written in the form of Eq. (21).

APPENDIX B: ANALYTIC AND ASYMPTOTIC RESULTS

We present explicit results for the additive cosine model (20) of the effective potential, with $0 \leq \kappa \leq 1$. The partial derivatives are then $w_\xi = -\sin \xi$ and $w_\eta = -\kappa \sin \eta$.

We consider first the symmetric case $\kappa = 1$ which, according to Eq. (6), can hold for all values of the magnetic

field only if the original modulation has square symmetry with equal lattice constants $a_x = a_y = a = 2\pi/K$ in both directions, so that $\Omega = (2\pi/a)^2 \tilde{V}_x / (m\omega_0)$.

Things become especially simple close to the maximum at the origin, where $w_\xi \approx -\xi$ and $w_\eta \approx -\eta$. Then the equipotentials become circles with radii $\rho_\epsilon = 4 - 2\epsilon$ independent of φ , and the Jacobian (A3) reduces to $\mathcal{J}_\epsilon = 1$. The angular velocity $d\varphi/dt = \Omega$ becomes constant along the equipotentials, and independent of ϵ . Thus, the GC motion in this approximation is very similar to the simple cyclotron motion, however with the circular frequency Ω instead of the cyclotron frequency ω_0 . As a consequence, all integrals in Eq. (A6) can easily be evaluated analytically, with the result

$$D_{xx}^{\text{cl},+}(\epsilon_{\text{qu}}) = \left(\frac{a}{2\pi}\right)^2 \frac{\Omega^2 \tau}{(2\pi)^2} \frac{\pi(2 - \epsilon_{\text{qu}})^2}{1 + (\Omega\tau)^2}, \quad (\text{B1})$$

where ϵ_{qu} is the energy above which the quadratic approximation is valid, and $D_{yy}^{\text{cl},+} = D_{xx}^{\text{cl},+}$, and $D_{yx}^{\text{cl},+} = -D_{xy}^{\text{cl},+} = \Omega\tau D_{xx}^{\text{cl},+}$. Thus, for $\Omega\tau \gg 1$, the motion of the GCs along closed equipotentials leads to a suppression $\propto (\Omega\tau)^{-2}$. For a suitable choice of $\epsilon_{\text{qu}} (= 2 - \sqrt{\pi} = 0.228)$ and a corresponding treatment of $D_{\mu\nu}^{\text{cl},-}$, one obtains the result indicated in Fig. 3 by the long-dashed line.

Going beyond this simple quadratic approximation, we obtain qualitatively similar results. All equipotentials with energy $\epsilon > 0$ (< 0) are closed lines around a maximum (minimum). As $|\epsilon|$ becomes small, the angular velocity varies along the orbits and becomes very small near the saddle points $[(\xi, \eta) = (0, \pi)$ and equivalent], where the Jacobian $\mathcal{J}_\epsilon(\varphi)$ diverges. Only the equipotentials exactly at $\epsilon = 0$ are open trajectories (straight lines), but they yield vanishing contribution to the diffusion tensor. Exploiting the symmetry, we can show that $D_{\mu\nu}^{\text{cl},+}$ and $D_{\mu\nu}^{\text{cl},-}$ of Eqs. (A6) yield identical contributions to the diagonal components of the diffusion tensor, whereas their contributions to the off-diagonal components cancel. The result for the non-vanishing diagonal components can be written as Eq. (17). The numerically calculated $\Phi(\Omega\tau)$ is plotted in Fig. 3. In the weak-modulation limit (or “dirty limit”, $\Omega\tau \rightarrow 0$) we have $\Phi(0) = 1$, as expected from Eqs. (12) and (15). For $\Omega\tau \rightarrow \infty$, $\Phi(\Omega\tau)$ becomes small. We can expand Eq. (A6) for large $\Omega\tau$ and show that the term linear in $1/\Omega\tau$ vanishes identically. The prefactor of the leading term can be calculated numerically, and we obtain $\Phi(\Omega\tau) \approx 3.29/(\Omega\tau)^2$ for $\Omega\tau \rightarrow \infty$. This can be used to obtain the one-parameter interpolation $\Phi_1(\Omega\tau) = 3.29/(3.29 + (\Omega\tau)^2)$, which approximates $\Phi(\Omega\tau)$ well for large values of $\Omega\tau$ (see Fig. 3). An apparent improvement at small and intermediate $\Omega\tau$ is obtained with the approximation $\Phi_3(\Omega\tau)$ defined in Eq. (18).

We now turn to the general rectangular symmetry. For $0 \leq \kappa < 1$ the equipotentials with energies $|\epsilon| \leq 1 - \kappa$ are open (in y direction), and degenerate into straight lines for $\kappa = 0$.

In the “dirty limit” $\Omega\tau \rightarrow 0$ the distinction between open and closed equipotentials is not relevant, since we can expand the velocity $v_\mu(t)$ into a Taylor series for small t and perform the integral in Eq. (8) term by term. Up to second order in $\Omega\tau$ we obtain

$$\Phi_{xx}(\Omega\tau, \kappa) = \kappa^2 [1 - (\Omega\tau)^2/2 + \dots], \quad (\text{B2})$$

$$\Phi_{yy}(\Omega\tau, \kappa) = 1 - \kappa^2(\Omega\tau)^2/2 + \dots, \quad (\text{B3})$$

for all values of κ .

In the “clean limit”, open equipotentials dominate $\Phi_{yy}(\Omega\tau, \kappa)$ and introduce a characteristic $\sqrt{\kappa}$ dependence for $\kappa \ll 1$. Already the fraction of the unit cell covered by open equipotentials, $A_{\text{open}}/(2\pi)^2 = 1 - A_{\text{closed}}^{\text{max}}/(2\pi^2)$, which is plotted versus κ (as dashed line) in Fig. 9, shows such a dependence. To see that, we calculated the corresponding area $A_{\text{closed}}^{\text{max}} = \int_{1-\kappa}^{1+\kappa} d\epsilon \int_{-\pi}^{\pi} d\varphi \mathcal{J}_\epsilon(\varphi)$ covered by closed equipotentials around a maximum (equal to that around a minimum), which allows the expansion $A_{\text{closed}}^{\text{max}} = 16\sqrt{\kappa} + O(\kappa^{3/2})$.

The contributions of closed equipotentials to both Φ_{xx} and Φ_{yy} vanish in the clean limit. The contribution of open equipotentials to $\Phi_{yy}(\infty, \kappa)$ is finite while that to $\Phi_{xx}(\infty, \kappa)$ vanishes, because the average value of the guiding center velocity component $v_y(t)$ is finite, while that of $v_x(t)$ is zero. Since $\Phi_{xx}(\Omega\tau, \kappa)$ behaves similar to $\Phi_{xx}(\Omega\tau)$ in the square-symmetric case, we extrapolated Eq. (B2) to arbitrary values of $\Omega\tau$ and found that Eq. (22) provides an extremely good approximation.

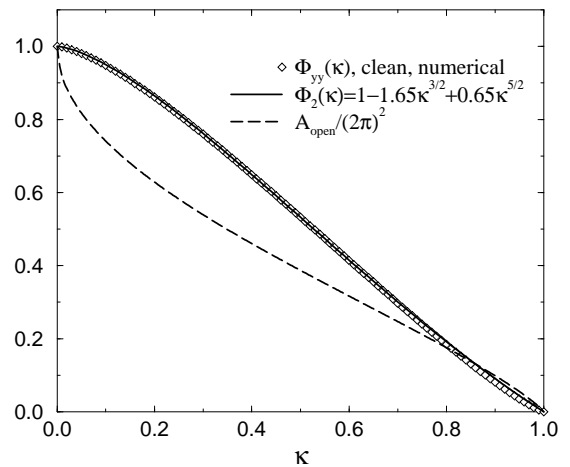


FIG. 9. Numerical result in the clean limit for $\Phi_{yy}(\infty, \kappa)$ (diamonds) versus anisotropy parameter $\kappa = \tilde{V}_y/\tilde{V}_x$, together with analytic approximation (solid line). Also shown is the fraction of the unit cell covered by open equipotentials (dashed).

Since, in the clean limit, $X = 1/(\Omega\tau) \rightarrow 0$, we can easily evaluate Eq. (A5) along an open equipotential, $W_x^-(-\varphi_\epsilon, \varphi_\epsilon; \epsilon) = -2\pi$, we obtain asymptotically from

Eq. (A7) $\Phi_{yy}(\infty, \kappa) = \int_{\kappa-1}^{1-\kappa} d\epsilon 4/(\Omega T_\epsilon)$ with

$$T_\epsilon = 2\mathbf{K}(q)/(q\Omega\sqrt{\kappa}), \quad q = (4\kappa/[(1+\kappa)^2 - \epsilon^2])^{1/2},$$

where $\mathbf{K}(q)$ is the complete elliptic integral²⁴. Expanding this for $\kappa \ll 1$, we obtain the leading terms $\Phi_{yy}(\infty, \kappa) \approx 1 - (31/6\pi)\kappa^{3/2}$. Adding a suitable term to satisfy $\Phi_{yy}(\infty, 1) = 0$, we obtained the approximation $\Phi_{yy}(\infty, \kappa) \approx \Phi_2(\kappa)$ as defined by Eq. (23). Apparently the plot in Fig. 9 reveals only for $\kappa \gtrsim 0.7$ slight deviations between exact and interpolated result.

Using Eq. (23) and the small $\Omega\tau$ expansion (B3), we tried to approximate $\Phi_{yy}(\Omega\tau, \kappa)$ by the one-parameter interpolation

$$\Phi_{yy}^{(1)}(\Omega\tau, \kappa) = \Phi_{yy}(\infty, \kappa) + [1 - \Phi_{yy}(\infty, \kappa)] / [1 + \beta_\kappa(\Omega\tau)^2], \quad (\text{B4})$$

with $\Phi_{yy}(\infty, \kappa) = \Phi_2(\kappa)$ and $\beta_\kappa = 0.5\kappa^2/[1 - \Phi_2(\kappa)]$. This yields a very good approximation for $\kappa < 0.5$, but a rather poor one for $\kappa \gtrsim 0.75$, and we improved it with the definition (24).

- ¹⁸ D. E. Grant, A. R. Long, and J. H. Davies, Phys. Rev. B **61**, 13127 (2000).
¹⁹ S. Chowdhury, C. J. Emeleus, B. Milton, E. Skuras, A. R. Long, J. H. Davies, G. Pennelli, and C. R. Stanley, Phys. Rev. B **62**, R4821 (2000).
²⁰ R. Fleischmann, T. Geisel, and R. Ketzmerick, Phys. Rev. Lett. **68**, 1367 (1992).
²¹ R. Schuster, K. Ensslin, J. P. Kotthaus, M. Holland, and C. Stanley, Phys. Rev. B **47**, 6843 (1993).
²² R. G. Chambers, in *The Physics of Metals, I: Electrons*, edited by J. M. Ziman, (Cambridge University Press 1969, London), p. 175.
²³ P. D. Ye, D. Weiss, R. R. Gerhardts, G. Lütjering, K. von Klitzing, and H. Nickel, Semicond. Sci. Technol. **11**, 1613 (1996).
²⁴ I. S. Gradshteyn and I. M. Ryzhik, *Table of Integrals, Series, and Products* (Academic Press, New York, 1994).

-
- ¹ D. Weiss, K. von Klitzing, K. Ploog, and G. Weimann, Europhys. Lett. **8**, 179 (1989), see also in *High Magnetic Fields in Semiconductor Physics II*, edited by G. Landwehr, Springer Series in Solid-State Sciences Vol. **87** (Springer-Verlag, Berlin 1989), p. 357.
² R. R. Gerhardts, D. Weiss, and K. von Klitzing, Phys. Rev. Lett. **62**, 1173 (1989).
³ R. W. Winkler, J. P. Kotthaus, and K. Ploog, Phys. Rev. Lett. **62**, 1177 (1989).
⁴ D. Weiss, K. von Klitzing, K. Ploog, and G. Weimann, Surf. Sci. **229**, 88 (1990).
⁵ H. Fang and P. J. Stiles, Phys. Rev. B **41**, 10171 (1990).
⁶ R. R. Gerhardts, D. Weiss, and U. Wulf, Phys. Rev. B **43**, 5192 (1991).
⁷ A. Lorke, J. Kotthaus, and K. Ploog, Phys. Rev. B **44**, 3447 (1991).
⁸ D. Weiss, A. Menschig, K. von Klitzing, , and G. Weimann, Surf. Sci. **263**, 314 (1992).
⁹ C. Zhang and R. R. Gerhardts, Phys. Rev. B **41**, 12850 (1990).
¹⁰ R. D. Hofstadter, Phys. Rev. B **14**, 2239 (1976).
¹¹ D. Pfannkuche and R. R. Gerhardts, Phys. Rev. B **46**, 12606 (1992).
¹² C. W. J. Beenakker, Phys. Rev. Lett. **62**, 2020 (1989).
¹³ S. D. M. Zworschke, A. Manolescu, and R. R. Gerhardts, Phys. Rev. B **60**, 5536 (1999).
¹⁴ R. R. Gerhardts, Phys. Rev. B **45**, 3449 (1992).
¹⁵ R. Menne and R. R. Gerhardts, Phys. Rev. B **57**, 1707 (1998).
¹⁶ R. R. Gerhardts, Phys. Rev. B **53**, 11064 (1996).
¹⁷ G. J. O. Schmidt, Phys. Rev. B **47**, 13007 (1993).